Microscale Thermophysical Engineering, 8:169–182, 2004

ISSN: 1089-3954 print/1091-7640 online
DOI: 10.1080/10893950490454928

Taylor & Francis
Taylor & Francis Group

INFRARED DIAGNOSTICS FOR MEASURING FLUID AND SOLID MOTION INSIDE SILICON MICRODEVICES

Gengxin Han, James C. Bird, K. Johan, A. Westin, Zhiqiang Cao, and Kenneth S. Breuer
Division of Engineering, Brown University, Providence, Rhode Island, USA

A new velocimetry system has been developed for use in microdevices that incorporate silicon as their structural material. The system is designed to illuminate and measure particle and surface motions using infrared wavelengths, taking advantage of the fact that silicon is largely transmissive to light with wavelength above 1 μm. The system allows the observation of motion inside silicon-based microdevices, which are otherwise opaque to light at visible wavelengths. By analyzing these images using both time-of-flight and phase-locked techniques, quantitative measurements are demonstrated concerning the position and speed of internal surfaces and the motion of fluids inside complex microfabricated devices. The system as demonstrated has a resolution of approximately 360 nm, although higher resolution is possible with future improvements.

Keywords infrared, PIV, motion detection

The rapid growth and significant progress in the development of microfluidic devices has revealed a need for measurement techniques to measure the flow inside microdevices with micron-scale resolution. Non-invasive diagnostics, such as Particle Image Velocimetry (PIV) [1] are well-suited to this task, and in recent years micro-PIV techniques have been described [2, 3] that press conventional methods to the limits of optical resolution. PIV is one example of a time-of-flight measurement, in which the velocity of an object is inferred by measuring its displacement during a known time period. The displacement is computed from two images, each exposed with a short laser pulse and taken in rapid succession. If the objects of interest are small particles suspended in a fluid, the velocity field can be measured. However, the technique is not restricted to suspended particles and can also be used on any feature that can be tracked in a pair of images. A second mode of measuring motion is by stroboscopic illumination of an object in harmonic motion. In general, this technique cannot be used for fluid motion because even if the flow is harmonic, suspended particles are unlikely to follow closed paths. However, this phase-locked technique has been used to great success in the measurement of the motion of harmonically forced MEMS devices such as accelerometers, et cetera [4].

Received 23 July 2003; accepted 3 February 2004.
This work was supported by DARPA and NSF. The authors acknowledge Carl Meinhart and Steve Wereley for many valuable discussions and the use of their PIV code, and Stu Jacobson and Alan Epstein for the use of a precious microengine bearing rig.
Address correspondence to Kenneth S. Breuer, Division of Engineering, Brown University, Box D, Providence, Rhode Island 02912, USA. E-mail: kbreuer@brown.edu

NOMENCLATURE

d_p	Physical particle diameter	x_c, y_c	Translation coordinates, corrected for rotation
d_e	Effect particle diameter	δt	Separation in time between adjacent exposures
d_s	Diffraction–limited spot diameter	λ	Wavelength of illuminating light
NA	Numerical aperture of imaging lens	θ	Image rotation angle
I	Intensity of received light		
M	Magnification		
x, y	Translation coordinates		

As the complexity of the microdevices increases, the ability to provide optical access through a transparent surface becomes increasingly difficulty to ensure. The use of transparent materials (glass, Pyrex, plastic, etc.) often represents a compromise to the fabrication sequence, as these materials are not as structurally or thermally robust as single-crystal silicon or silicon carbide and cannot be processed with as much flexibility as is available for silicon-based substrates. In addition, the fabrication methods for these materials tend to be less precise, compromising precision fabrication. Finally, as multi-layer microfabricated silicon structures become increasingly common, the requirement to incorporate a glass window for visualization purposes is often impossible to accommodate without further complication to the fabrication sequences—a complication that is usually unacceptable.

Although visible light is no longer suitable as an illumination source for a micro-PIV system, the absorption coefficient of silicon falls sharply in the near-infrared regime and is effectively transparent at wavelengths between 1.1 and 2.5 μm. This property implies that infrared (IR) light might be a desirable illuminating source for PIV system if one would like to visualize motion inside a silicon-based microdevice. The present article explores the idea of using IR illumination to measure motion inside silicon devices.

BACKGROUND THEORY

In Figures 1 and 2 the device is illuminated using a twin Nd:YAG laser system, which emits a pair of 4.5-ns pulses at 1064 nm. Although we could use this wavelength, the transmissivity of silicon is not optimal here, and higher wavelengths are more desirable. To achieve this, the beam is frequency-doubled to 532 nm and then directed through an opto-parametric-oscillator (OPO)—a nonlinear optical system that enables the laser pulse to be tuned to a wavelength anywhere between 300 nm and 2000 nm. In the present case, we typically tune the laser to 1200 nm, where silicon reaches a high level of transparency. The pulse is then coupled to a fiber-optic delivery system and directed to the target, which is flood-illuminated by the two laser pulses. The angle at which the light hits the target is quite important and depends on what is being illuminated. For solid surface measurement, we have found that illumination in pure transmission mode is the most effective, in which case the laser is positioned directly below the sample, at ninety degrees to the focal plane. For small particle illumination typical of PIV, an angle of approximately 25 degrees with respect to the optical axis was found to be optimal (this is discussed in more detail later).

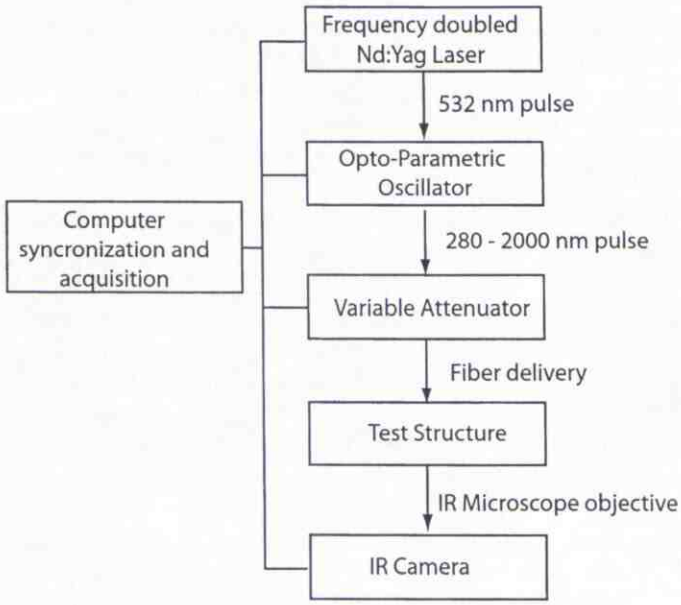

Figure 1. Overall schematic of IR micro motion system.

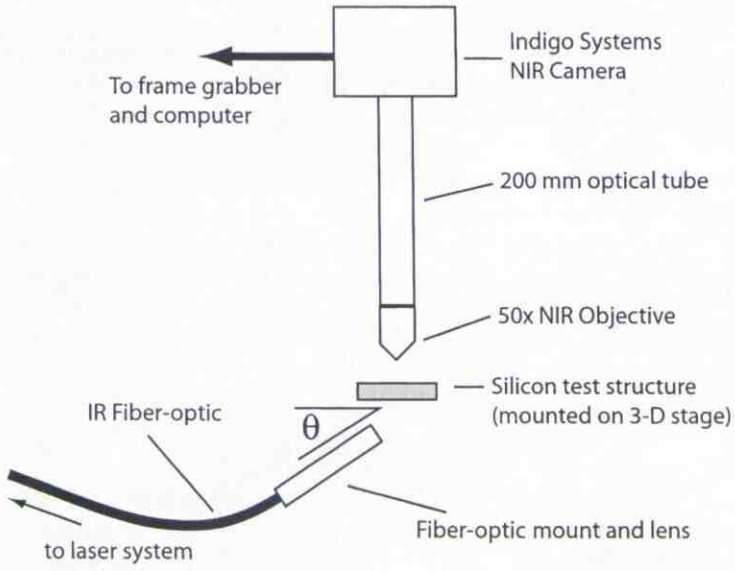

Figure 2. Schematic of the optical configuration for micro-motion measurement.

The scattered light is collected by a near-infrared (NIR) microscope objective mounted on a 200 mm corrected tube and imaged using an Indigo Systems Indium Gallium Arsenide (InGaAs) NIR camera. This camera has a 320 × 256 pixel array (30-μm pixel size) with excellent sensitivity between 900 and 1700 nm. Different microscope objectives have been used for different studies. For PIV measurements, a 50x, 0.42 NA Mititoyo objective has been used. This optical arrangement gives a field of view of 192 × 154 μm, which, although small, gives good resolution of the small particles that are imaged in PIV measurements. For the solid surface motion study described in this article, a 20x, 0.3 NA objective was used to achieve a larger field of view (at the cost of spatial resolution).

The resultant images are transferred at 60 Hz to a data acquisition computer. Although the NIR camera is a video-rate device and cannot be triggered, as can most modern CCD systems, the laser pulses are synchronized to the video sync signal and can be adjusted to fall anywhere within the video frame. In the case of phase-locked operation, the position of the laser pulse in the frame is not important, as long as it does not fall on the inter-frame boundary, in which case a dead image will result. However, in the case of time-of-flight measurements, the laser timing is adjusted so that the two laser pulses straddle adjacent video frames. For the Indigo camera, this inter-frame boundary is 0.12 ms in duration, so that the separation between the two laser flashes can be no shorter than 0.12 ms—more than adequate for most low-speed motions. Higher speed activity can be captured either with dual-illumination of a single frame or by using two cameras externally synchronized to be out of phase. Triggered IR cameras or interline cameras, which can store two images in quick succession, may be available in the near future to ease this concern.

FLUID VELOCITY MEASUREMENTS

A significant difference between visible micro-PIV and the IR micro-PIV system is the particle scattering technique used. In a visible PIV system, one can use an inelastic technique, such as epi-fluorescence, to image submicron particles. This has the advantage that background reflections at the excitation wavelength can be filtered out by the use of a dichroic filter, greatly enhancing the sensitivity of the image-gathering optics and enabling the use of small particles, which can track the flow very accurately. In contrast, in the IR system fluorescent particles with both absorption and emission bands in the IR regime do not exist (to our knowledge), and this mandates the use of elastic scattering techniques to image the particles. Laser scattering from small particles is highly dependent on the particle size and wavelength, and the scattered intensity (I) varies like [3, 5]:

$$I \propto d_p^6/\lambda^4$$

where d_p is the particle diameter and λ is the wavelength of the recording light, from which we see that there is a tradeoff between higher wavelengths to achieve greater silicon transmissivity and greater sensitivity in the NIR camera (which also increases at higher wavelengths), and using lower wavelengths to maximize the scattering intensity and to improve the point spread function size. A compromise wavelength of 1200 nm was found to work well. The intensity penalty due to wavelength can also be offset by using particles of larger diameter d_p.

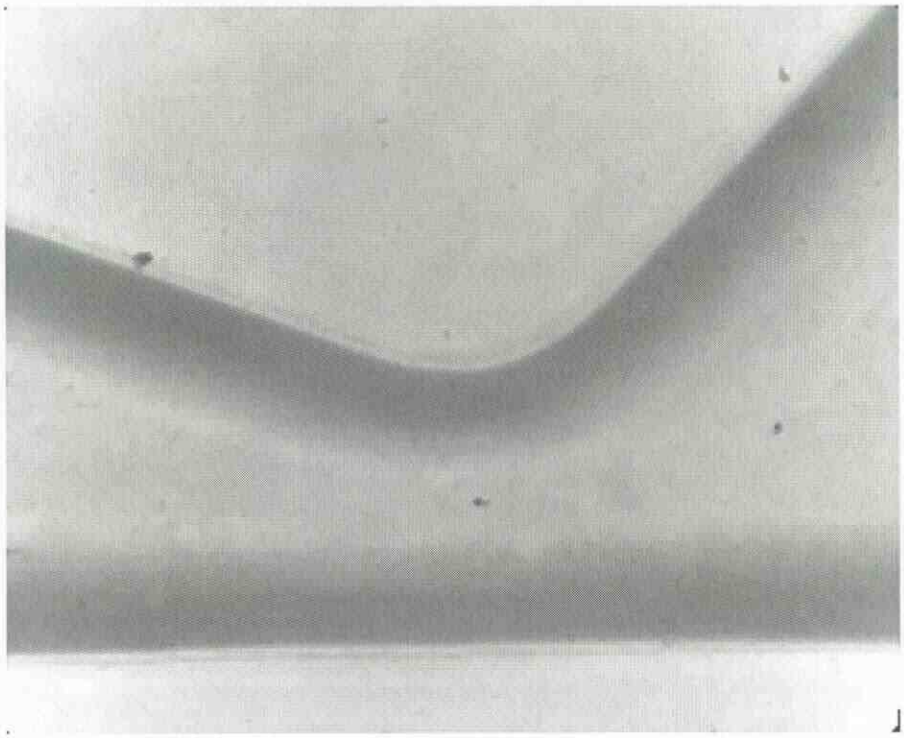

Figure 3. IR image of micronozzle throat using broad band illumination without flow. The shadows are due to the diffraction in the silicon-air transition. The PIV images are taken on the right side of the image, near the lower wall.

The geometry tested was a converging-diverging flow inside a silicon micronozzle, shown in Figure 3. The device was fabricated by etching the nozzle geometry 300 μm deep into a 500 micron-thick silicon wafer. A second silicon wafer was fusion-bonded to the first in order to cap the structure. The device is thus opaque to visible light. The nozzle shown in Figure 3 has a throat width of 40 μm. The measurements reported here were taken downstream of the throat where the flow expands to a channel 300 μm deep by 1000 μm wide.

The water flow was seeded (0.06% by volume) with 1 μm uncoated polystyrene particles with a refractive index of 1.56. The relative refractive index is 1.17 (compared to water). Smaller particles would be preferable, but the intensity increases strongly with particle diameter (see above), and this was found to give good particle visibility.

As mentioned above, elastic scattering must be used in the IR due to the absence of fluorescent tracers at this wavelength. In order to maximize the visibility of particles, a simple darkfield system was implemented in which the laser light was brought in at high incidence angle as indicated in Figure 2. The undeflected beam enters the focal plane at an angle too high to be captured by the microscope objective and thus the majority of the image is dark. However, a particle in the light path will deflect the beam due to the mismatch between the polystyrene bead's index of refraction and that of the surrounding water. The efficiency of this illumination system was tested using beads

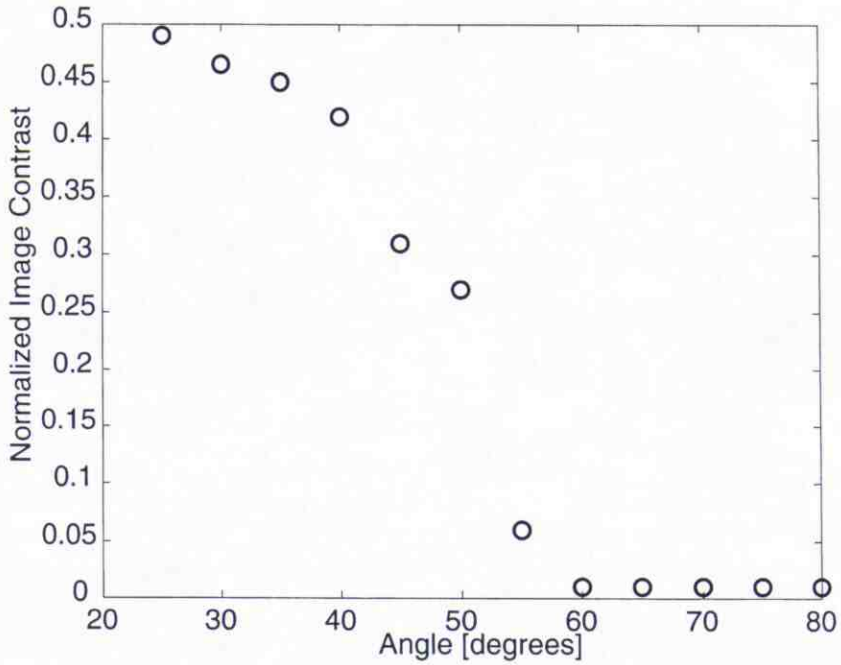

Figure 4. Normalized contrast as a function of laser illumination angle (referenced to optical axis). For each case, optimum laser intensity is used.

evaporated onto a silicon wafer and then measuring the image contrast resulting from different illumination angles. The results are shown in Figure 4. At low angles (direct illumination), the light intensity entering the camera is too high, resulting in image saturation; above the critical angle of the lens (in this case about 18 degrees) good image contrast is achieved. As the angle increases, too little of the light is scattered from the particles into the microscope objective and the image contrast degrades. A sample image of the polystyrene beads suspended in water and illuminated using this protocol is shown in Figure 5. The individual tracer particles are clearly visible. In common with other micro-PIV images, out-of-focus particles are visible as a background "glare."

In a micro-PIV system, the spatial resolution of the system is given by the diameter of the diffraction-limited point spread function, d_s, in the image plane, which is given by:

$$d_s = 2.44M\frac{\lambda}{2NA}$$

where M is the total magnification of the microscope, and NA is the numerical aperture of the objective lens [2, 3]. At a wavelength of 560 nm, with a 1.4 NA 60× objective, Santiago et al. report $d_s = 29.3$ μm [3]. For the same lens system (which will operate in the near IR, as long as it is not anti-IR coated), but using light at 1.2 μm, this is degraded to 62 μm. For the 50×, 0.42 NA objective used in the current study, the point-spread diameter is 174 μm. This is considerably larger than the optimal lens system and is primarily due to the low NA of the current lens. However, the low NA has a significant

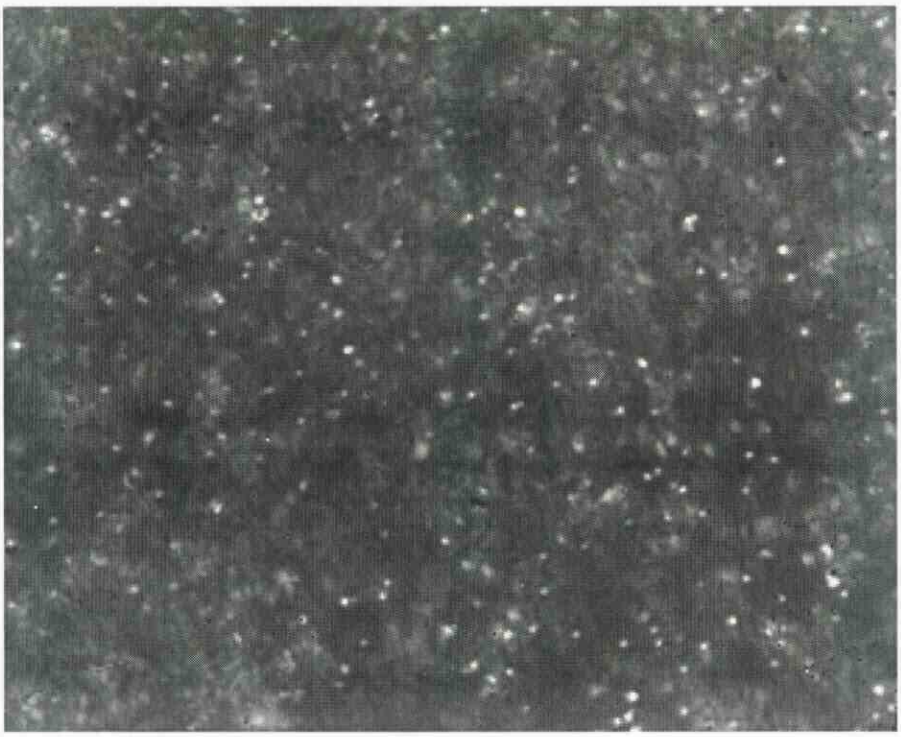

Figure 5. Sample image of tracer particles suspended in water, illuminated using IR laser pulse (1200 nm). The picture measures 320 × 256 pixels and field of view is 194 μm × 154 μm.

advantage—it has a large working distance, which is important for imaging inside thick silicon devices and convenient for this proof-of-concept study.

If we track a 1 μm particle, then, following Adrian [1] and Meinhart et al. [2], the effective diameter, d_e, projected on the image plane can be expressed as

$$d_e = (M^2 d_p^2 + d_s^2)^{1/2}$$

which yields $d_e = 181$ μm, compared with approximately 30 μm reported by Meinhart et al. [2] for visible light micro-PIV. The spot size is dominated by the diffraction point spread. However, since the NIR camera has large pixel sizes (30 μm), this is not as bad as it seems, and the imaged particle is only six pixels wide—close to ideal for PIV sub-pixel interpolation. Assuming that we can achieve one-tenth pixel accuracy in the PIV algorithms, this gives a spatial resolution of 360 nm.

In the current experiment, by using two pulse separation times ($\delta t = 0.125$ ms and 17.5 ms), we measured the velocity in two flow conditions: a) a high-flow-rate regime where the average nozzle throat velocity is 62 mm/s, and b) a low-flow-rate regime where the average nozzle throat velocity is 250 μm/s. The interrogation areas chosen were a region close to the wall (for the high-speed flow condition) and a region away from walls in the nozzle expansion (for the low-speed flow condition). These are simply representative regimes, and no attempt was made to map the entire flow field at this time.

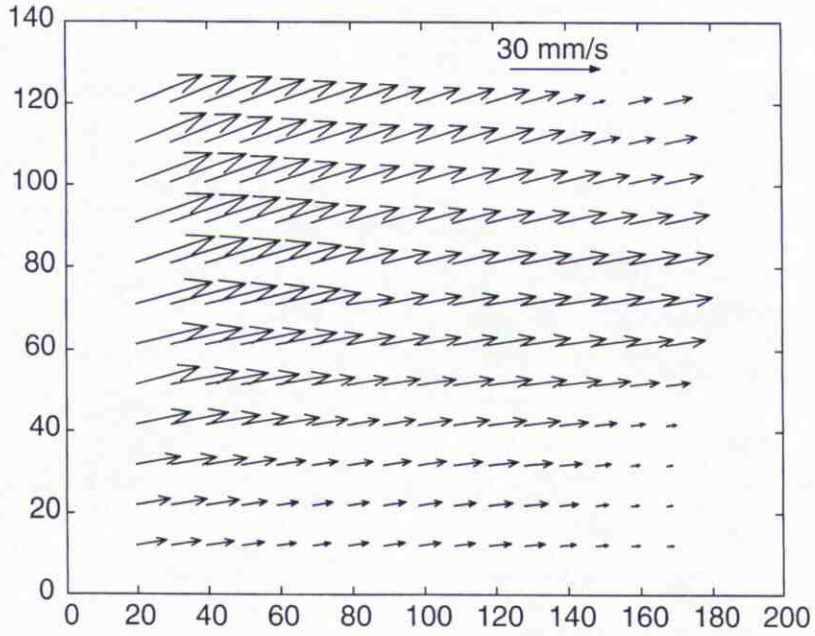

Figure 6. Velocity vectors inside the micronozzle. The lower part of the test area is close to the nozzle wall. The axis coordinates are in μm.

The image pair was analyzed using in-house PIV processing techniques, and selected results were confirmed using well-tested custom micro-PIV software [6]. The in-house PIV data processing techniques are based on the MATLAB-based image analysis software developed by Sveen [7] and modified to include the cross-correlation signal-to-noise ratio as a criterion during the ensemble averaging of velocity vectors. In processing the average, we first set an acceptable value of signal-to-noise ratio (SNR) and only pick up the vector whose correlation satisfies the SNR threshold participating in the average. The typical number of measurements included in an average is about 40 and only 7% of the total vectors were rejected due to poor SNR. The vector fields for the high speed condition are shown in Figure 6, computed using an interrogation window size of 64×64 pixels and by overlapping the interrogation windows by 75%. The lower axis represents the location of the solid wall where the velocity is zero. The focal plane is in the middle of the nozzle, away from either the upper or lower nozzle boundaries. The dynamic range of the system (the ratio of the highest resolved speed to the lowest resolved speed) is limited by the pixel resolution of the images.

SOLID SURFACE MOTION MEASUREMENTS

The IR micromotion system can also be used for detection of the position and velocity of a solid feature inside the silicon structure. If the motion of the solid object is harmonic, we can operate in "phase-locked" mode, in which the laser is locked to the frequency of the device (or some precisely controlled detuned frequency). This has been amply demonstrated by Freeman [4] using visible light and by our own group,

using IR illumination [8]. If, however, the motion of the solid object is not harmonic, there is no phase reference and a time-of-flight measurement technique similar to the PIV technique is necessary. This is demonstrated using the rotation of a microturbine, fabricated as part of the MIT Microengine program [9]. The rotor consists of a 4-mm turbine disk, shown in Figure 7, which can rotate in a stationary housing (supported by an air bearing). The completed microturbine is a complex device and is comprised of five silicon wafers bonded in a stack with the rotor forming the middle layer. The entire device (Figure 7, right) is encased by silicon and is not accessible to visible light, save for a small access hole for a fiber-optic speed sensor. One motivation for imaging the rotation is to determine both the speed of rotation and (more importantly) to image the details of any subsynchronous motion ("whirl"), which can lead to rotor instabilities and, ultimately, to failure.

Figure 8 shows a pair of images of the moving rotor taken using the laser illumination while it is spinning at low speed (approximately 6000 rpm). In the time-of-flight (or PIV) mode, the lasers are fired in rapid succession, and in this case the two flashes are separated by 150 microseconds. The motion of the rotor is clearly visible. In order to analyze this image pair both the translation and rotation of image B with respect to image A must be computed. The pictures are first cleaned up by removing dead pixels and overexposed pixels either by thresholding the image (re-assigning pixels that have values that are below or above a given value) or by using a median filter or an adaptive Wiener filter, both designed to remove high frequencies and "salt and pepper" noise. The images are also equalized so that their intensity distributions are matched.

The velocity of a feature in the image is determined as follows: A first-guess interrogation area (IA) is first selected on each image (Figure 8). This area should contain well-defined features that will be easy to track. Edges and other high-contrast features are most desirable. In addition, features that are highly non-isotropic (i.e., have clear orientation) are preferable in order to compute image rotation. In the example shown in Figure 8, the leading edge of the rotor blade is selected as the interrogation area. The images are next linearly de-trended, windowed (using a Hamming window), and cross-correlated using an FFT-based cross-correlation routine.

The cross-correlation for the image pair shown in Figure 8 is presented in Figure 9. Notice that there is a well-defined peak whose position indicates the best-fit translation of the image. This peak is interpolated to sub-pixel accuracy by fitting the cross-correlation near the maximum to a Gaussian surface (with arbitrary orientation and aspect ratio). Using this translation data, Image B is translated using a spline-based sub-pixel interpolation routine. In addition, a circular ring image is interpolated from the original Cartesian-based pixel grid, again using spline interpolation. A one-dimensional cross-correlation in the azimuthal direction is performed on the ring image to determine the image rotation. As with the translational computation, Gaussian sub-pixel interpolation is used to optimize the rotation between the two images. The azimuthal cross-correlation is performed for several radial values, and the median rotational angle is chosen as the optimal image rotation. Image B is rotated using a bicubic interpolation, and the interrogation areas are re-computed. The entire process is repeated iteratively until no further improvement is observed.

For the second rotation and beyond, a translational error is introduced by the rotation step. The error is due to the center of rotation not corresponding to the center of the image. Since the true center of rotation is not known, we instead chose an arbitrary

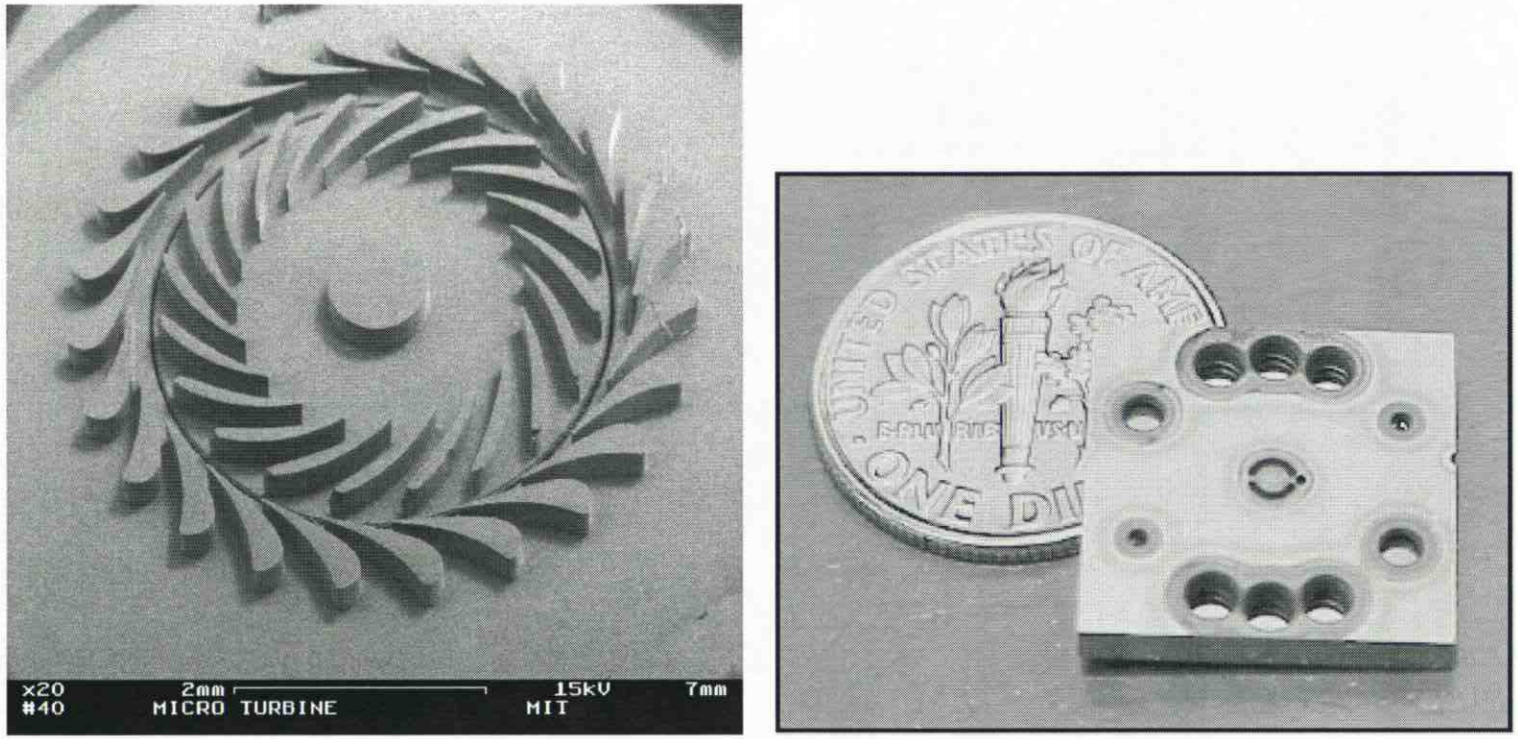

Figure 7. Photograph of microrotor (left) and its enclosing package (right). The blades on the turbine are imaged by the IR motion system as it rotates in the bearing. The enclosing package consists of silicon wafers both above and below the rotor plane, thus preventing visible light imaging of the rotor (images reproduced from Fréchette et al. [9]).

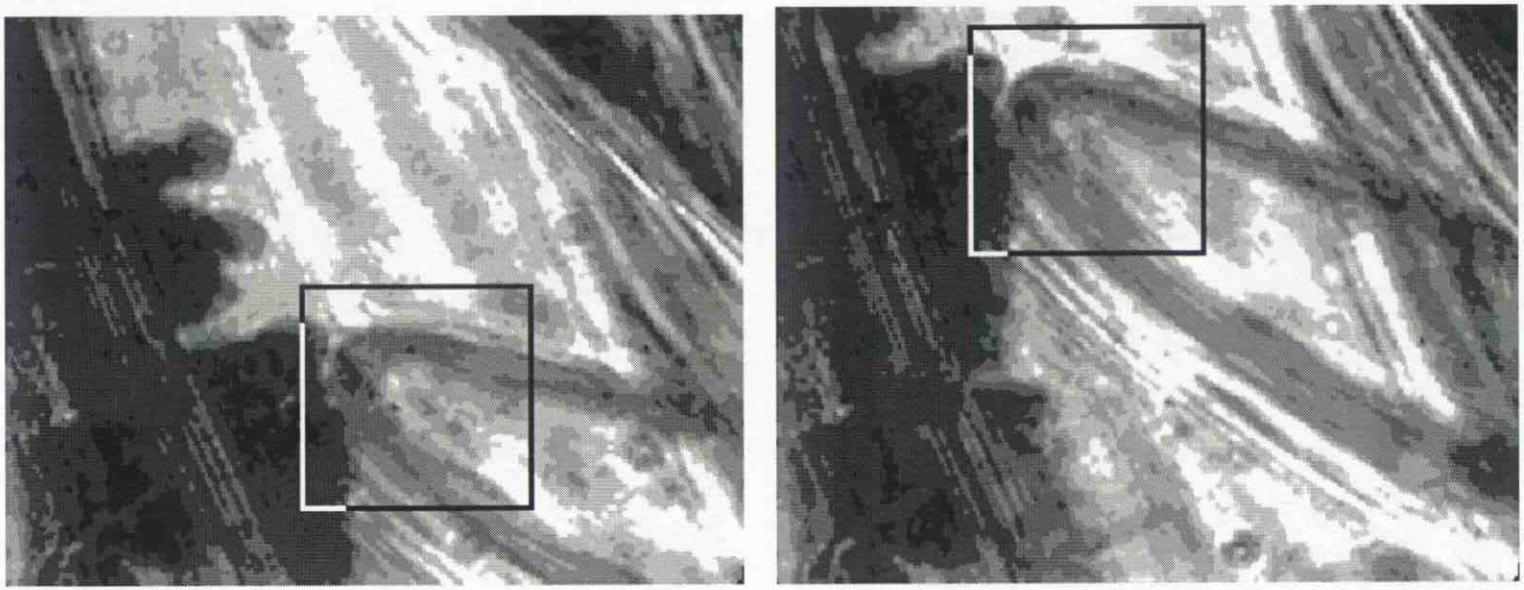

Figure 8. Pair of IR images taken using laser illumination, of a buried microrotor as it spins inside its rotor bearing. The size of each image is 480 × 384 (μm). The square boxes in each frame represent the initial interrogation areas used to compute translation and rotation.

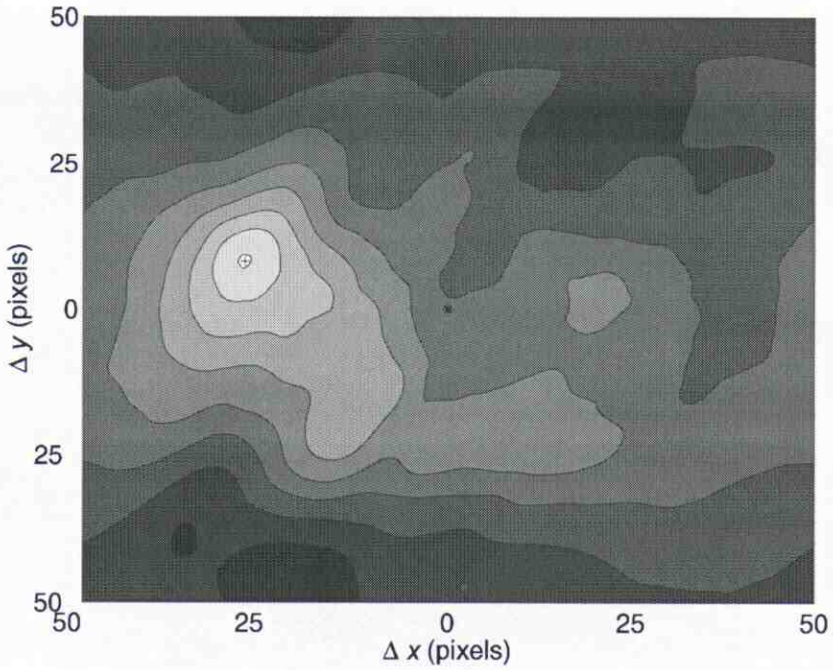

Figure 9. Shaded contour plot of the cross-correlation obtained during the (first) translation phase. Note the well-defined maximum indicating the optimal translation.

reference point within the interrogation area (IA). For convenience, the center of the first IA is used. As long as we always rotate about this point, no translational error is introduced. However, implementing the algorithm in this manner is both cumbersome (in terms of coding), and, more importantly, has some operational disadvantages. The solution is to always rotate the image about the center of the current IA (which changes from one iteration to the next) and to correct for the translation induced by the difference between the image center and the IA center. The correction is given by:

a) when x and y have the same sign:

$$x_c = \frac{2|x|}{x}\sqrt{x^2+y^2}\sin\left(\frac{\theta}{2}\right)\cos\left(\frac{(\pi-\theta)}{2}-\tan^{-1}\frac{y}{x}\right)$$

$$y_c = -\frac{2|y|}{y}\sqrt{x^2+y^2}\sin\left(\frac{\theta}{2}\right)\sin\left(\frac{(\pi-\theta)}{2}-\tan^{-1}\frac{y}{x}\right)$$

b) when x and y have different signs:

$$x_c = \frac{2|y|}{y}\sqrt{x^2+y^2}\sin\left(\frac{\theta}{2}\right)\sin\left(\frac{(\pi-\theta)}{2}-\cot^{-1}\frac{y}{x}\right)$$

$$y_c = \frac{2|x|}{x}\sqrt{x^2+y^2}\sin\left(\frac{\theta}{2}\right)\cos\left(\frac{(\pi-\theta)}{2}-\cot^{-1}\frac{y}{x}\right)$$

where x and y are the previous translation and θ is the rotation.

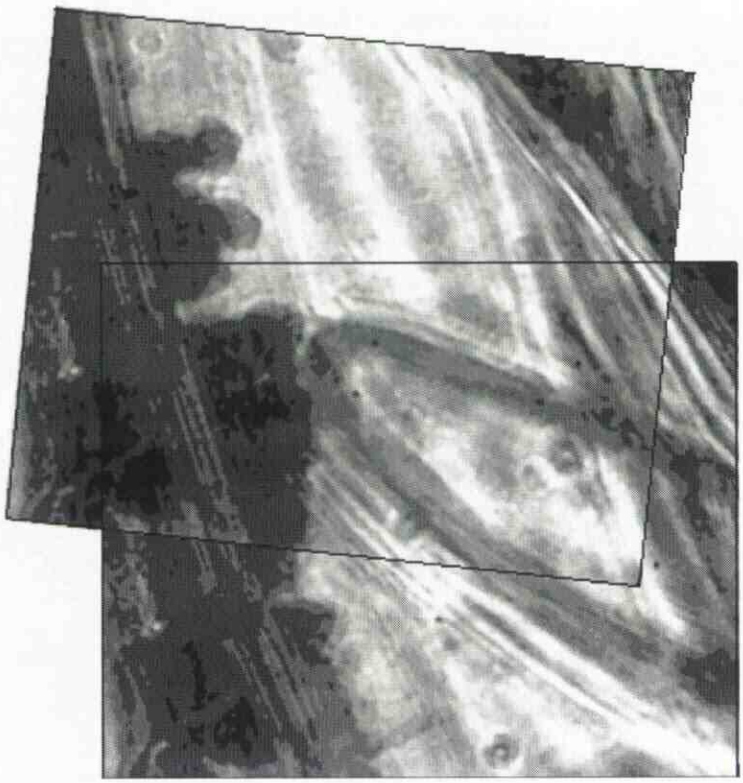

Figure 10. Microrotor image pair, translated, rotated, and superimposed, indicating the optimal image shift. In this case $\Delta x = -44.1$, $\Delta y = -111.4$ (pixels) and $\Theta = 5.1$ degrees.

The results of the completed translation/rotation operation are shown in Figure 10, which shows the previous image pair superimposed after the optimal translation and rotation. For a perfect image pair, we find that the process is accurate to better than 0.02 pixels and 0.02 degrees, although image-to-image noise does degrade this performance.

CONCLUSIONS

An IR micro-motion system designed to illuminate and measure particle and surface motions inside silicon micromachined devices using infrared wavelengths has been developed and demonstrated. The system has a resolution of approximately 360 nm, although this can be improved by a factor of 2 with high NA optics. Although the resolution is not as good as visible-light micro-PIV systems (due to the longer wavelength, the need for larger focal length optics, and limits in current IR imaging technologies), it is more than adequate for many micro flows and motions of interest, particularly since other means of interrogation inside the structure are not possible. The system can also be used for imaging inside silicon carbide structures, which are also transparent in the IR. The system is now being extended to incorporate more sophisticated motion algorithms, as well as to measure instabilities, mixing, and reactions inside complex silicon devices.

REFERENCES

1. R. J. Adrian, Particle-Imaging Techniques for Experimental Fluid Mechanics. *Annual Review of Fluid Mechanics*, vol. 23, pp. 261–301, 1991.
2. C. D. Meinhart, S. T. Wereley, and J. G. Santiago, PIV Measurements of a Microchannel Flow. *Experiments in Fluids*, vol. 27, pp. 414–419, 1999.
3. J. G. Santiago, S. T. Wereley, C. D. Meinhart, D. J. Beebe, and R. J. Adrian, A Particle Image Velocimetry System for Microfluids. *Experiments in Fluids*, vol. 25, pp. 316–319, 1998.
4. D. Freeman, Measuring Motions in MEMS. *Materials Research Soc.* Bulletin. vol. 26, pp. 305–306, 2001.
5. M. Born and E. Wolf, Principles of Optics, Sixth Edition, Cambridge University Press, Cambridge, 1997.
6. S. T. Wereley, Personal communication, Purdue University, 2000.
7. J. K. Sveen, *MatPIV 1.4*, Mechanics Division, Department of Mathematics, University of Oslo, Norway, 2000.
8. K. S. Breuer, J. C. Bird, G. Han, and K. J. Westin, Infrared PIV for Measurement of Fluid and Solid Motion in Micromachined Devices, *Proc. ASME IMECE*, New York, November 2001.
9. L. Fréchette, S. A. Jacobson, K. S. Breuer, F. E. Ehrich, R. Ghodssi, R. Khanna, C.-W. Wong, X. Zhang, M. A. Schmidt, and A. H. Epstein, Demonstration of a Microfabricated High-Speed Turbine Supported on Gas Bearings, *Proc. IEEE Solid State Sensors and Actuators Workshop*, Hilton Head, SC, June 2000.
10. C. D. Meinhart, S. T. Wereley, and M. H. B. Gray, Volume Illumination for Two-Dimensional Particle Image Velocimetry. *Measurement Science and Technology*, vol. 11, pp. 809–814, 2000.